NJC

Accepted Manuscript

This is an *Accepted Manuscript*, which has been through the Royal Society of Chemistry peer review process and has been accepted for publication.

Accepted Manuscripts are published online shortly after acceptance, before technical editing, formatting and proof reading. Using this free service, authors can make their results available to the community, in citable form, before we publish the edited article. We will replace this *Accepted Manuscript* with the edited and formatted *Advance Article* as soon as it is available.

You can find more information about *Accepted Manuscripts* in the Information for Authors.

Please note that technical editing may introduce minor changes to the text and/or graphics, which may alter content. The journal's standard Terms & Conditions and the Ethical guidelines still apply. In no event shall the Royal Society of Chemistry be held responsible for any errors or omissions in this *Accepted Manuscript* or any consequences arising from the use of any information it contains.

ROYAL SOCIETY OF CHEMISTRY

www.rsc.org/njc

Journal Name

ARTICLE

A universal strategy for the facile synthesis of sandwich-structured Pt-graphene-Pt nanocomposite for Salbutamol sensing

Received 00th January 20xx,
Accepted 00th January 20xx

DOI: 10.1039/x0xx00000x

www.rsc.org/

Xiaofei Zhu [a,b,†], Xuemin Duan [a,†], Jingkun Xu [a,*], Limin Lu [b,*], Kaixin Zhang [c], Huakun Xing [a], Yansha Gao [a], Taotao Yang [a], Wenmin Wang [b]

In this work, sandwich-structured Pt-graphene-Pt (P-Gr-P) nanocomposite has been prepared by two-step method including (i) a chemical and (ii) an electrochemical reduction process. P-graphene oxide-P (P-GO-P) nanocomposite was firstly synthesized by an in situ growth method, during which Platinum nanoparticles (PtNPs) grew on both sides of GO. In the second step, P-GO-P was modified onto glass carbon electrode (GCE), GO in P-GO-P nanocomposite was reduced to a more conductive form of graphene (Gr). The obtained sandwich-structured P-Gr-P can effectively separate the individual layers of Gr sheets from each other, prevent the agglomeration of Gr sheets and improve the conductivity of the Gr film. In addition, the electrocatalytic properties of the as prepared P-Gr-P nanocomposite towards the oxidation of salbutamol (SAL) were investigated. Results revealed that the sandwich-structured P-Gr-P nanocomposite with higher electrochemically active surface area showed better electrocatalytic activity toward SAL oxidation than PtNPs-Gr prepared by using one-step electrochemical co-deposition method. On the basis of the excellent electrochemical activity of P-Gr-P nanocomposite, a highly sensitive electrochemical platform was developed for the rapid detection of SAL. The present work provides an interesting strategy to prepare Gr-based nanocomposite for electrochemical sensors.

1. Introduction

Salbutamol [1-(4-hydroxy-3-hydroxymethylphenyl)-2-(t-butylamino)ethanol] (SAL) is a β_2 adrenergic receptor agonist which primarily used in the treatment of bronchial asthma and other forms of allergic airway disease associated with respiratory pathway[1]. SAL is also applied as a tocolytic agent in humans as well as in veterinary medicine. However, residues of SAL in higher doses may display lipolytic effect and toxic to humans[2]. Therefore, it is necessary to establish quick and accurate methods to detect SAL residues. Electrochemical methods have been proved to be ideal methods for the analysis of drugs and related compounds because of their high accuracy, sensitivity, low cost and easy operation[3,4]. A key role played in electrochemical detection should be the modified electrode materials, which determines the sensitivity and speed of response to a large extent. However, to the best of our knowledge, only a few reports in literatures involved the detection of SAL by using modified GCE, and the linear range and detection limit need to be improved. Therefore, development electrochemical method for detection of SAL with improved performance is significant.

Gr, a single-atom-thick sheet arranged in honey comb structure, has gained enormous attention due to its large specific surface area, superior mechanical properties and remarkable electronic conductivity[5-7]. The applications of Gr have been reported in various fields such as batteries[8], supercapacitors[9], chemical sensors and biosensors[10-12]. However, Gr easily tends to form irreversible agglomerates or even restock to form graphite due to the π-π interaction between individual Gr[13]. To solve this problem, the preparation of Gr-based composites, including carbon nanotubes-Gr composites[14,15], biomaterials-Gr composites[16,17], Gr-polymer composites[18-20] and Gr-metals composites[21-23], is considered to prevent the aggregation of Gr sheets. Especially, the design and synthesis of Gr-metal nanohybrids are of great interest both for fundamental studies and for potential nanodevice applications[24,-27]. It is well realized that the dispersion of metal nano-particles on Gr sheets would potentially provide a new way to develop novel catalytic, magnetic, and optoelectronic materials[28].

As a kind of noble metal, platinum (Pt) has been applied in many catalytic fields due to its unusual physical and chemical properties, such as sensors[29], fuel cells electrocatalysts[30] and counter electrodes in the dye-sensitized solar cells[31]. It has been reported that PtNPs-Gr can display a synergic effect of catalytic characters of both Gr and PtNPs, in which Gr can give rise to an extraordinary modification to the PtNPs and PtNPs deposited on Gr accelerated the electron transfer[32]. To date, varieties of methods have been developed to synthesis PtNPs-Gr composites, such as chemical method[33], microwave synthesis[34] and electrochemical technique[35]. Among these methods, electrochemical method has attracted a

[a] School of Pharmacy, Jiangxi Science and Technology Normal University, Nanchang 330013, PR China. E-mail: xujingkun@tsinghua.org.cn. Tel.: +86 791 8537967; Fax: +86 791 3823320
[b] College of Science, Jiangxi Agricultural University, Nanchang 330045, PR China. E-mail: lulimin816@hotmail.com
[c] Centre for Nanoscale BioPhotonics, Macquarie University, North Ryde, 2109, NSW, Australia. Email: kaixin.zhang@mq.edu.au
† These authors contributed equally to this work and should be considered co-first authors.

Electronic Supplementary Information (ESI) available: The cycle stability and long-term stored stability of P-Gr-P/GCE. See DOI: 10.1039/x0xx00000x

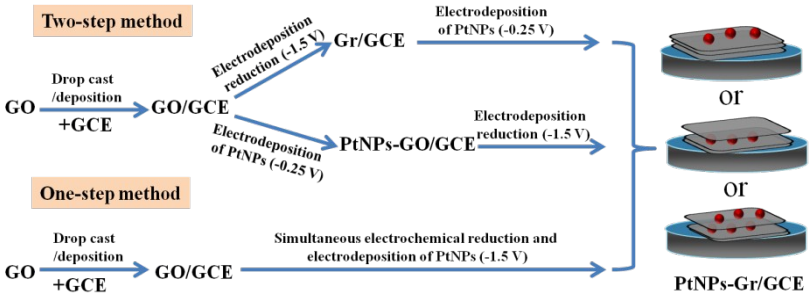

Scheme 1 The two-step and one-step methods for the synthesis of PtNPs-Gr/GCE.

lot of interest due to its simple operation, eco-friendly, mild conditions and size controllable. Typically, two types of strategies have been proposed to electrochemically deposit PtNPs on Gr, including two-step and one-step electrochemical methods (Scheme 1). In the two-step method, GO is drop-cast or deposited on the electrodes, and then GO or Gr-coated electrodes are immersed in a metallic precursor solution to perform electrochemical reduction at negative potential or in reverse order. While in the one-step method, simultaneous electrochemical reductions of H_2PtCl_6 and GO are performed. However, the above-mentioned methods for PtNPs-Gr synthesis lack control over the distribution of PtNPs. In addition, the aggregation of Gr is still unable to avoid because there are large amounts of free GO sheets assembled on the surface of electrode or in the electrolysis solutions during the electrochemical reduction process.

More recently, several research groups[36,37] have reported that metal NPs can be strongly anchored onto the GO surface by mixing GO and a metallic precursor aqueous solution without applying any additional reductants or surfactants, during which GO acted as both stabilizer and reductant. They found that the resultant metal NPs can be uniformly dispersed on both surfaces of GO. Inspired by these pioneering works, in this article, a novel sandwich-structured P-Gr-P nanocomposite was synthesized, and was firstly used as the active material for the fabrication of electrochemical SAL sensor. The P-Gr-P nanocomposite was prepared by two-step method including (i) a chemical and (ii) an electrochemical reduction process. In the first step, P-GO-P nanocomposite was synthesized through a simple in situ growth method, in which GO can successfully reduce H_2PtCl_6 to PtNPs and PtNPs grew on both sides of GO. The monolayer GO can be effectively isolated by PtNPs and forming sandwich structure in the solution. In the second step, the as prepared P-GO-P nanocomposite was coated on the GCE and experienced an electrochemical process. In this process, GO was reduced to Gr and the P-Gr-P nanocomposite was obtained. The sandwich-structure of P-Gr-P can effectively prevent the agglomeration of Gr and improve conductivity of the composite**.** Furthermore, the as-prepared P-Gr-P was used as sensing material for the sensitive detection of SAL. The sensing performances of the P-Gr-P toward SAL oxidation were investigated. Satisfied results demonstrated that the P-Gr-P nanocomposite with high electrochemical active surface area showed enhanced electrochemical signal toward the oxidation of SAL. This work has expanded the scope of synthesizing Gr-based hybrid and explored their sensing applications.

2. Experimental

2.1. Chemicals and reagents

SAL was purchased from Aldrich. SAL stock solution (5×10^{-3} M) was prepared with absolute ethanol and stored at 277-281 K. GO was obtained from Nanjing Xianfeng nano Co. $H_2PtCl_6{\bullet}3H_2O$, disodium hydrogen phosphate dodecahydrate (Na_2HPO_4), and sodium dihydrogen phosphate dehydrate (NaH_2PO_4) were purchased from Sinopharm chemical reagent Co. Ltd. Other reagents were of analytical grade, double distilled water was used during the experiments.

2.2. Instrumentation

SEM images were obtained at Helios NanoLab FESEM/FIB. TEM images were obtained at TecnaiG2 T2 transmission electron microscope. UV/vis spectra analysis was performed using a Perkin-Elmer Lambda 900 ultraviolet-visible-near-infrared spectrophotometer (Germany). Raman spectroscopy (invia-reflex) was used to analyze the samples using a 633 nm laser. Electrochemical measurements including cyclic voltammetry, differential pulse voltammetry and electrochemical impedance spectroscopy techniques were carried out on CHI 660D electrochemical workstation (Shanghai, China). The measurement was carried out in a three-electrode system, including GCE or composites modified GCE as working electrode, platinum wire as auxiliary electrode and saturated calomel reference electrode (SCE). During the experiments, the atmosphere of double distilled water was set by passing N_2 for 15 min.

2.3. Material preparation

Synthesis of P-GO-P: GO was dispersed in double distilled water and ultrasonic treatment for 3 h to obtain a concentration of 0.5 mg mL^{-1}. Subsequently, the PtNPs/GO was prepared by mixing 0.5 mg/mL GO aqueous solution with 7.9 mM H_2PtCl_6 at a ratio of 10:1 (v/v) and reacted under vigorous stirring at 80 ℃ for 24 h[37]. The obtained product was named as P-GO-P.

Preparation of sandwich like P-Gr-P and fabrication of P-Gr-P composite modified electrode: Before modification, GCE was mechanically polished using chamois leather containing 0.05 μm Al_2O_3, and then it was ultrasonically cleaned with double distilled water, absolute ethanol and double distilled water, respectively, each for 5 min. The cleaned GCE was dried with a nitrogen stream prior to the subsequent modification.

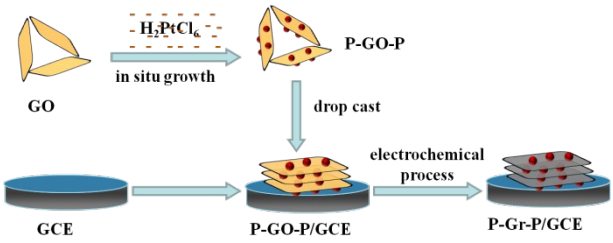

Scheme 2 The preparation process of P-Gr-P/GCE.

To obtain P-Gr-P modified GCE (P-Gr-P/GCE), 5 μL P-GO-P dispersion was dropped on the surface of GCE and dried at room temperature. The P-GO-P/GCE was transferred to an electrochemical cell containing 0.1 M phosphate buffer solution (PBS) (pH 7.0). GO in P-GO-P composite film was electrochemically reduced to Gr by performing successive cyclic voltammograms for 400 s in a potential window between -1.5 to 0 V, and the scan rate was set as 50 mV s^{-1}. The preparation process was shown in Scheme 2. For comparison, Gr modified GCE (Gr/GCE) and GO modified GCE (GO/GCE) were also prepared.

3. Results and discussion

3.1. Characterization of P-Gr-P

The morphology and structure of Gr and P-Gr-P were characterized by SEM and TEM. The samples of Gr and P-Gr-P on indium tin oxide (ITO) glasses were prepared by an electrochemical method. Briefly, GO or P-GO-P dispersion was dropped on the ITO surface and dried, and then GO/ITO or P-GO-P/ITO was transferred to an electrochemical cell and reduced by performing successive cyclic voltammograms for 400 s in a potential window between -1.5 to 0 V. As can be seen from Fig. 1A, a typical wrinkled structure with the corrugation and scrolling is intrinsic to Gr. For P-Gr-P nanocomposite (Fig. 1B), one can see that a large amount of PtNPs were uniformly distributed on the surface of Gr. In addition, the structure of Gr and sandwich-structured P-Gr-P were further confirmed by TEM techniques. As shown in Fig. 1C, Gr displayed a layered stacking structure. This structure easily tended to agglomeration due to the decrease of oxygen-containing functional groups after experienced an electrochemical process. By contrast, it can be observed from Fig. 1D that the P-Gr-P nanocomposite contained three layers of Gr, where Gr layers were regularly spaced by layers of PtNPs. Since PtNPs were distributed on both sides of Gr layer, the sandwich structure of P-Gr-P can effectively avoid aggregation. The sandwich structured nanocomposite could extremely enhance the active surface area, allow the analyte (here SAL) to fully touch the PtNPs, and provide enough space for mass transfer of reactants and products. Consequently, the resulting modified electrode would exhibit an excellent electrocatalytic capability towards the oxidation of SAL.

Raman spectroscopy is one of the most effective techniques to characterize the ordered and disordered crystal structures of Gr. Therefore, Raman spectroscopy was used to characterization of Gr based materials. In particular, samples of GO and P-GO-P were dropped on ITO surface without conducting electrochemical reduction process. Fig. 2A shows Raman spectra of GO, Gr, P-GO-P and P-Gr-P composites. Raman spectra usually shows two peaks (G band and D band), the G band was corresponding to the sp^2-hybridized carbon atoms in the hexagonal framework and the D band was the oxidation of disruption of the sp^2-hybridized carbon atoms. The D/G band intensity ratio (I_D/I_G) in the Raman spectrum expresses the atomic ratio of sp^2/sp^3 carbons, and is a measure of the extent of disordered graphite. As can be seen in Fig. 2, GO displayed a D band at 1315 cm^{-1} and a G band at 1590 cm^{-1}. While Gr showed a G band at 1570 cm^{-1}, and the I_D/I_G was up to 1.18 (0.98 for GO). This phenomenon can be explained that the distortion of 6-fold rings caused by oxygen functionalities is removed after GO deoxidation[38], and the carbon lattice returns to an essentially graphitic state with highly defected, resulting in the increase of I_D/I_G ratio[39]. For P-GO-P, the I_D/I_G (1.01) increased slightly as compared with GO, indicating the successfully growth of PtNPs on Gr defects[40]. As for P-Gr-P, the I_D/I_G increased to 1.21, higher than P-GO-P or Gr. The increased I_D/I_G can be attributed to the reduction process altered the structure of GO in P-GO-P, and the presence of PtNPs deter the recovery of the sp^2 carbon domain and decrease the G band intensity of Gr[40,41].

The reduction process was demonstrated by UV-vis absorption spectra and the results are shown in Fig. 2B. It can be found that the UV-vis spectra of GO (a) and P-GO-P (c) exhibited two characteristic peaks, one was at 229 nm corresponding to $\pi \rightarrow \pi^*$ transitions of aromatic C-C bonds, and the other at 300 nm was attributed to $n \rightarrow \pi^*$ transitions of C=O bonds[42]. After the electrochemical reduction process, the peak at 229 nm was red shifted to 246 nm (Fig. 2B, b and d), which was an indication of the restoration of the electronic conjugation within the Gr sheets[43]. The results of UV-vis spectra indicated that the electrochemical reduction of GO indeed took place.

Electrochemical impedance spectroscopy (EIS) is widely used to study the interface properties of the modified electrode. The impedance spectrum includes two parts, a semicircle diameter at higher frequencies corresponds to the electron-transfer resistance (R_{et}) and a linear part at lower frequencies corresponds to the diffusion process. Fig. 2C shows the results of EIS of bare GCE (a), GO/GCE (b), Gr/GCE (c) and P-Gr-P/GCE (d) in the presents of 5 mM $[Fe(CN)_6]^{3-/4-}$ containing

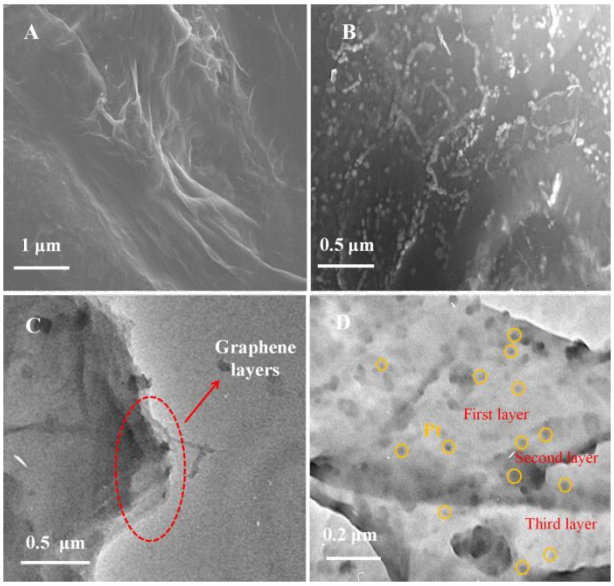

Fig. 1 SEM images of Gr (A), P-Gr-P (B) and TEM images of Gr layer (C), sandwich structure of P-Gr-P (D).

0.1 M KCl at scan rate of 50 mV s^{-1}. It was observed that bare GCE displays a R_{et} of 500 Ω. While the R_{et} of GO/GCE was 4900 Ω, possibly due to the poor conductivity of GO. However, dramatically decreased R_{et} value can be found when Gr was modified on GCE, which was attributed to the excellent electronic property of Gr, forming a fast electron conduction pathway between the electrode and the electrochemical probe. As for P-Gr-P/GCE, the semicircle in the plot became much smaller than that of electrode without PtNPs. The excellent conductivity was probably due to the fact that PtNPs accelerated the electron transfer and the sandwich structure of P-Gr-P can effectively prevent Gr from agglomerating.

3.2. Electrochemical behaviour of SAL on P-Gr-P/GCE

To evaluate the electrochemical performence of P-Gr-P, P-Gr-P/GCE was characterized by cyclic voltammetry in the presence of SAL in the potential range from 0.3 V to 0.9 V. Fig. 3 presents typical cyclic voltammograms of bare GCE

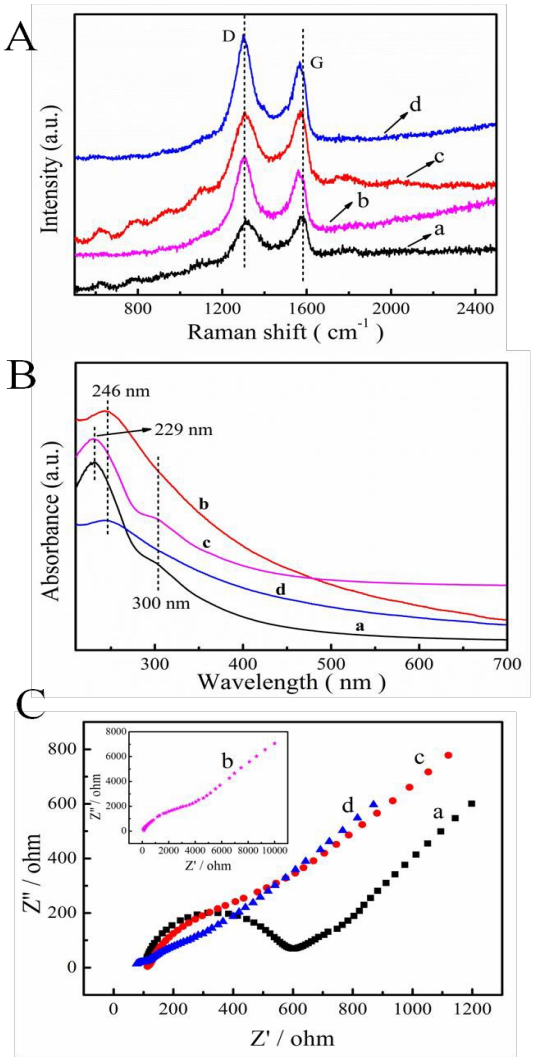

Fig. 2 (A) Raman spectra of GO (a), Gr (b), P-GO-P (c) and P-Gr-P (d). (B) UV-vis absorption spectra of GO (a), Gr (b), P-GO-P (c) and P-Gr-P (d). (C) The impedance spectrum of bare GCE (a), GO/GCE (b), Gr/GCE (c) and P-Gr-P/GCE in 5 mM $Fe(CN)_6^{3-/4-}$ (1:1) solution containing 0.1 M KCl. Scan rate: 50 mV s^{-1}.

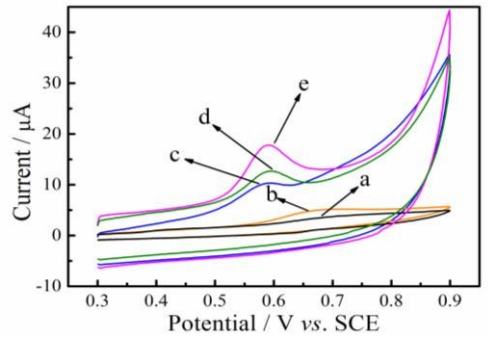

Fig. 3 Cyclic voltammograms of 20 μM SAL in 0.1 M PBS (pH 7.0) at bare GCE (a), GO/GCE (b), Gr/GCE (c) PtNPs-Gr/GCE (d) and P-Gr-P/GCE (e). Scan rate: 50 mV s^{-1}.

(curve a), GO/GCE (curve b), Gr/GCE (curve c), PtNPs-Gr/GCE (curve d) and P-Gr-P/GCE (curve e) in pH 7.0 PBS containing 20 μM SAL. As can be seen, no obvious redox peak can be observed at bare GCE, which might be due to the sluggish electron transfer of GCE (curve a). While GO/GCE exhibited a slightly obvious oxidation peak current response, possibly due to the fact that GO hold strong adsorption capacity, but exhibited poor conductivity (curve b). However, as shown in Fig. 3 (curve c), the oxidation peak current as well as background current increased significantly at Gr/GCE, ascribing to the excellent conductivity and large surface area of Gr. Larger oxidation peak current can be observed on PtNPs-Gr/GCE, which was prepared by one-step electrodeposition method, indicating PtNPs distributed on Gr surface improved the electrochemical oxidation of SAL (curve d). As for P-Gr-P/GCE, the oxidation peak current increased again, which was three times higher than that at Gr/GCE (curve e). Moreover, it also can be seen that the oxidation peak current of SAL at the sandwich-structured P-Gr-P electrode was much higher than that at the PtNPs-Gr/GCE, adding to evidence that the special sandwich structure of P-Gr-P showed better performance as compared to ordinary PtNPs-Gr composites. Therefore, the excellent electrochemical catalytic properties of P-Gr-P can be summarized in the following three aspects: firstly, Gr has good electrical conductivity and large specific surface area, which can provide an excellent microenvironment for the catalytic oxidation of SAL. Secondly, the well-distributed PtNPs on the surface of Gr with a high density would provide more active sites for the catalytic oxidation reaction and greatly increase the electrocatalytic activity. Thirdly, for the sandwich-structure of P-Gr-P, SAL molecules can rapidly diffuse from the solution into the nano-P-Gr-P modified membranes.

3.3. Optimization of the experimental conditions

Accumulation can improve the amount of SAL absorbed on the electrode surface, and then improve sensitivity determination. Then, the influence of accumulation time was investigated. As can be seen from Fig. 4A, the influence of accumulation time ranging from 10 to 90 s on the oxidation of SAL at P-Gr-P/GCE was investigated. It was observed that the oxidation current response increased sharply with increasing the reduction time from 10 s to 60 s, and then reached a constant limiting value, which demonstrated that the adsorption of SAL was fast and easily reached saturation on P-Gr-P/GCE. Based on the sensitivity and short analysis time, 60 s accumulation time was chosen in subsequent experiments.

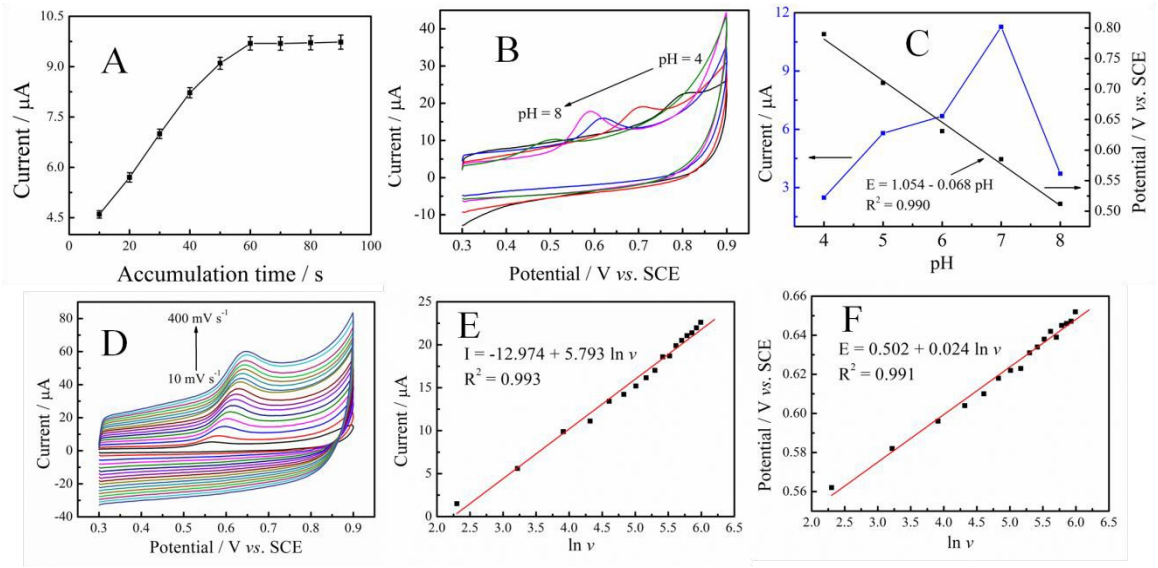

Fig. 4 (A) Variation of the peak current with accumulation time in 0.1 M PBS (pH 7.0). SAL concentration: 20 μM. Scan rate: 50 mV s^{-1}. (B) Cyclic voltammograms of P-Gr-P/GCE in PBS with different pH containing 20 μM SAL. (C) Effect of pH value on the anodic peak potentials and anodic peak currents of SAL. (D) Cyclic voltammograms of 20 μM SAL with different scan rates (v) on P-Gr-P/GCE in 0.1 M PBS (pH 7.0) (from the inner to the outer are 10, 25, 50, 75, 100, 125, 150, 175, 200, 225, 250, 275, 300, 325, 350, 375 and 400 mV s^{-1}, respectively.). Accumulation time: 60 s. (E) Linear relationship of anodic peak current I versus the natural logarithm of v. (F) The relationship between E_p and natural logarithm of v.

Fig. 4B shows the effect of pH of the supporting electrolyte on electro-oxidation of 20 μM SAL at P-Gr-P/GCE in 0.1 M PBS with a scan rate of 50 mV s^{-1}. As can be seen, with the increase of pH value, the oxidation potential (E_{pa}) of SAL shifted toward less positive values, suggesting the involvement of proton in the oxidation reaction[44]. The plot of the peak potential *vs.* pH showed one straight line between pH 4 and 8 and it can be expressed by the following equation (Fig. 4C):

$$E_{pa} = 1.054 - 0.068\ pH\ (R^2 = 0.990)$$

The slope of the above equation was -68 mV pH^{-1}, which was close to -59 mV pH^{-1}, indicating the equal numbers of proton and electron involved in electrode reaction. In addition, it was also found that the peak current increased with the pH from 4.0 to 7.0, and then decreased from 7.0 to 8.0. Therefore, pH 7.0 was employed for further studies.

The kinetics of the electrode reaction was investigated by studying the effects of scan rate on the oxidation of SAL at the P-Gr-P/GCE. As shown in Fig. 4D, with the increase of the scan rate, the anodic peak currents also increased. The anodic peak currents increased linearly with the natural logarithm of scan rates (ln v) from 10 mV^{-1} to 400 mV^{-1} (Fig. 4E), corresponding to the following equation: I (μA) = -12.974 + 5.793 ln v (R^2 = 0.990), suggesting that electrode process of SAL was diffusion-controlled[45]. Similarly, a linear relationship between E_{pa} and ln v was also observed in the range of 10 – 400 mV s^{-1} (Fig. 4F), and the linear regression equation can be expressed as E_{pa} = 0.502 + 0.024 ln v (R^2 = 0.991). According to the following equation[46]:

$E_{pa} = E^{0'} + (RT/\alpha nF)\ [0.780 + \ln(D_R^{1/2}/k^0) + \ln(\alpha nFv/RT)^{1/2}] = K + (RT/2\alpha nF)\ \ln v$

where $E^{0'}$ is the formal potential, k^0 is the standard heterogeneous rate constant, α is transfer coefficient of the oxidation of SAL, D_R is diffusion coefficient of SAL, other symbols have their usual significance. The value of αn can be calculated to be 0.53 from the slope. Generally, α is assumed

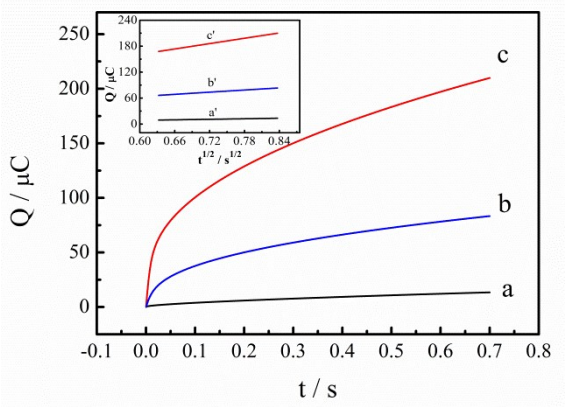

Fig. 5 (A) Plot of Q-t curves of bare GCE (a), PtNPs-Gr/GCE prepared by one-step electrodeposition method (b) and P-Gr-P/GCE (c) in 0.1 mM $K_3[Fe(CN)_6]$ containing 1.0 M KCl. Insert: Plot of Q-$t^{1/2}$ curves on bare GCE (a'), PtNPs-Gr/GCE (b') and P-Gr-P/GCE (c').

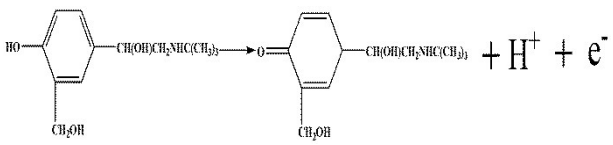

Scheme 3 Chemical structure of SAL and its oxidation mechanism at P-Gr-P/GCE.

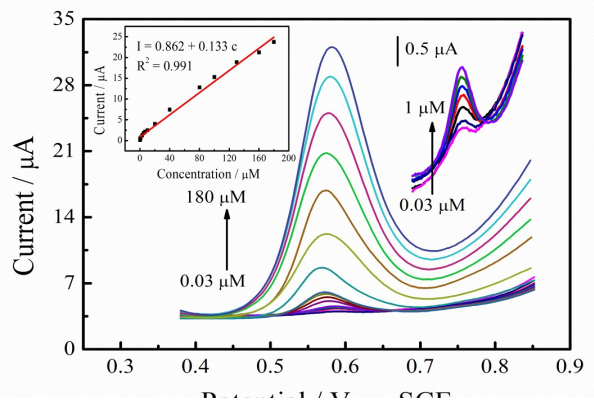

Fig. 6 Differential pulse voltammograms of 0.03, 0.07, 0.2, 0.4, 0.6, 0.8, 1, 3, 5, 7, 10, 20, 40, 80, 100, 130, 160, and 180 μM SAL on P-Gr-P/GCE in 0.1 M PBS (pH 7.0) at the scan rate of 50 mV s^{-1}. Insert: plot of the oxidation peak current against the concentration of SAL.

as 0.5 in the totally irreversible electrode process. Therefore, one electron is involved in the oxidation of SAL. In summary, SAL takes place a one-electron, one-proton irreversible reaction (shown in Scheme 3).

3.4. Chronocoulometry

The electrochemically effective surface areas (A) of bare GCE (Fig. 5, curve a), PtNPs-Gr/GCE (prepared by one-step electrodeposition) (Fig. 5, curve b) and P-Gr-P/GCE (Fig. 5, curve c) have been investigated. According to the previous literature[47], A can be determined by chronocoulometry using 0.1 mM $K_3[Fe(CN)_6]$ containing 1 M KCl as model complex, based on Anson equation:

$$Q(t) = 2nFAcD^{1/2}t^{1/2}/\pi^{1/2} + Q_{dl} + Q_{ads}$$

where Q_{ads} is the Faradic charge, Q_{dl} is the double-layer charge, D_0 is the diffusion coefficient (the diffusion coefficient of $K_3[Fe(CN)_6]$ in 1 M KCl is 7.6 × 10^{-6} cm^2 s^{-1}), c is the concentration of the substrate, and A is the surface area of the working electrode. Other symbols have their usual meanings. The linear regression equation of Q-$t^{1/2}$ curves on GCE (Inset of Fig. 5, curve a′), PtNPs-Gr/GCE (Inset of Fig. 5, curve b′) and P-Gr-P/GCE (Inset of Fig. 5, curve c′) were Q (10^{-6} C) = -3.670 + 20.394 $t^{1/2}$ (R^2 = 0.999), Q (10^{-6} C) = -13.762 + 73.182 $t^{1/2}$ (R^2 = 0.999) and Q (10^{-6} C) = 37.596 + 205.990 $t^{1/2}$ (R^2 = 0.999), respectively. Based on the slopes of the linear relationship between Q and $t^{1/2}$, A was calculated to be 0.068 cm^2 for bare GCE, 0.244 cm^2 for PtNPs-Gr/GCE. While the A of P-Gr-P/GCE was 0.682 cm^2, 10 times larger than that of bare GCE and 3 times larger than that of PtNPs-Gr/GCE. These results indicated that P-Gr-P sandwich structure showed a large surface area, which could increase the electrochemical active site, enhance the electrochemical response and decrease the detection limit.

3.5. Determination of SAL on P-Gr-P/GCE

Under the optimal experimental conditions established above, the calibration curves of SAL in PBS were measured by differential pulse voltammetry (DPV). Fig. 6 shows the typical differential pulse voltammograms obtained from different SAL concentrations at P-Gr-P/GCE. As can be seen, the peak current was proportional to the concentration of SAL over 0.03 to 180 μM range with the regression equation of I (μM) = 0.862 + 0.133 c (R^2 = 0.991) (Inset of Fig. 6). The detection limit was down to 9 nM (S/N = 3). Simultaneously, the comparison of P-Gr-P/GCE with other modified electrodes for SAL determination was also listed in Table 1. It can be seen that P-Gr-P/GCE was more sensitive with a wider linear range and lower detection limit. These results indicate that P-Gr-P/GCE is an appropriate platform for the determination of SAL.

Table 1 Comparison of the proposed sensor for determination of SAL with others

Electrode	Methods	Linear range (μM)	Detection limit (μM)	Reference
	CV[a]	0.1-0.3		
SWCNT-NF[1]/GCE	LSV[b]	0.3-3.3	0.1	[48]
	DPV[c]	3.3-33.3		
NGITO[2]	OSWV[d]	0.21-8.36*	0.31*	[49]
PTCPE[3]	CV	2.5-47.5	0.025	[50]
MWNT[4]/GCE	SWV[e]	0.8-10	0.7	[51]
P-Gr-P/GCE	DPV	0.03-180	0.009	This work

1 single-walled-multi-walled and nafion composites
2 nano gold particles modified indium tin oxide
3 pre-treated carbon paste electrode
4 multi-carbon nanotubes
a cyclic voltammetry
b linear sweep voltammetry
c differential pulse voltammetry
d osteryoung square wave voltammetry
e square wave voltammetry
* The linear range and detection limit in the literature is 50-2000 ng/ml and 75 ng/ml, respectively, equal to 0.21-8.36 μM, 0.31 μM, respectively.

Table 2 Recovery measurements of the SAL in the urine samples using P-Gr-P modified GCE

Samples	Added (μM)	Found (μM)	*RSD (%)	Recovery (%)
1	0	0	-	-
2	0.02	0.019	2.3	95.0
3	0.10	0.105	1.6	105.0
4	0.18	0.177	2.1	98.3
5	2.6	2.51	1.9	96.5
6	8.4	8.33	2.5	99.2

*RSD (%) calculated from six separate experiments.

3.6. Stability and reproducibility

The stability of P-Gr-P/GCE was verified by recording successive cyclic voltammograms in a potential range of 0.3 - 0.9 V. No obvious change could be observed in cyclic voltammograms after 10 cycles (current signal change less than 2 %) and the electrodes also remained stable in the presence of SAL up to 20 successive cycles (current change less than 4 %) (Fig. S1), which indicated P-Gr-P/GCE exhibited very stability. Furthermore, no significant change of the oxidation currents can be observed (current change less than 3.06 %) after the electrodes have been stored at room temperature for more than 30 days (Fig. S2), indicating the sensor has acceptable reproducibility and repeatability.

3.7. Real sample analysis

Furthermore, the proposed sensor was applied to the determination of SAL in urine samples. Urine samples were obtained from health volunteers, which were diluted 50-fold with 0.1 M PBS (pH 7.0) and centrifuged at 5000 rpm for 5 min to remove the suspended particles. The analytical applicability of the sensor was evaluated by determining the recoveries of six target samples with different concentrations by the standard addition method. As can be seen in Table 2, the results were satisfactory with a recovery in the range from 95.0% to 105.0%, indicating that the proposed method can be successfully applied in the detection of SAL concentration in urine sample.

Conclusions

In summary, a simple two-step approach has been developed for the preparation of the Pt-graphene-Pt composite with a novel sandwich-like structure. Pt nanoparticles not only acted as a spacer between graphene sheets to prevent aggregation, but also accelerated the electron transfer. Pt-graphene-Pt modified GCE showed a good performance for sensitive determination of salbutamol due to its excellent electronic conductivity and large specific surface area. Under optimized conditions, the Pt-graphene-Pt modified glass carbon electrode exhibited a good performance in terms of low limit of detection (9 nM) and wide linear range (0.03 - 180 μM), it also exhibited good stability, repeatability and reproducibility. These results indicate that the novel sandwich-like structure of Pt-graphene-Pt is scientifically interesting and has great potential for use in sensors, nanoelectronics, and other electrochemical applications.

Acknowledgements

We are grateful to the National Natural Science Foundation of China (51272096 and 51302117), the Natural Science Foundation of Jiangxi Province (20122BAB216011 and 20151BAB203018), Jiangxi Provincial Department of Education (GJJ13258), Postdoctoral Science Foundation of China (2014M551857 and 2015T80688), Postdoctoral Science Foundation of Jiangxi Province (2014KY14) and the Science and Technology Landing Plan of Universities in Jiangxi province (KJLD14069 and KJLD12081) for their financial support of this work.

Notes and references

1 C. X. Guo, H. B. Yang, Z. M. Sheng, Z. S. Lu, Q. L. Song, C. M. Li, *Angew. Chem. Int. Ed.*, 2010, 49, 3014.
2 X. Jia, J. Campos-Delgado, M. Terrones, V. Meunier, M. S. Dresselhaus, *Nanoscale*, 2011, 3, 86.
3 S. A. Ozkan, B. Uslu, P. Zuman, *Anal. Chim. Acta*, 2002, 457, 265.
4 B. Uslu, S. A. Ozkan, *Electrochim. Acta*, 2004, 49, 4321.
5 A. K. Geim, K. S. Novoselov, *Nat. Mater.*, 2007, 6 183.
6 C. Lee, X. D. Wei, J. W. Kysar, J. Hone, *Science*, 2008, 321, 385.
7 R. F. Service, *Science*, 2009, 324, 875.
8 E. Yoo, J. Kim, E. Hosono, H. S. Zhou, T. Kudo and I. Honma, *Nano Lett.*, 2008, 8, 2277.
9 S. Chen, J.W. Zhu, X.D. Wu, Q.F. Han and X. Wang, *ACS Nano*, 2010, 4 2822.
10 L. M. Lu, H. B. Li, F. L. Qu, X. B. Zhang, G. L. Shen, R. Q. Yu, *Biosens. Bioelectron.*, 2011, 26, 3500.
11 L. Zhang, Y. P. Wen, Y. Y. Yao, Z. F. Wang, X. M. Duan, J. K. Xu, *Chinese Chem. Lett.*, 2014, 25, 517.
12 F. L. Qu, T. Li, M. H. Yang, *Biosens. Bioelectron.*, 2011, 26, 3927.
13 Y. Si, E. T. Samulski, *Chem. Mater.*, 2008, 20, 6792.
14 V. C. Tung, L. M. Chen, M. J. Allen, J. K. Wassei, K. Nelson, R. B. Kaner and Y. Yang, *Nano Lett.*, 2009, 9, 1949.
15 Z. J. Fan, J. Yan, L. J. Zhi, Q. Zhang, T. Wei, J. Feng, M. L. Zhang, W. Z. Qian and F. Wei, *Adv. Mater.*, 2010, 22, 3723.
16 C. H. Lu, H. H. Yang, C. L. Zhu, X. Chen and G. N. Chen, *Angew. Chem. Int. Ed.*, 2009, 121, 4879.
17 H. X. Chang, L. H. Tang, Y. Wang, J. H. Jiang and J. H. Li, *Anal. Chem.*, 2010, 82, 2341.
18 T. Ramanathan, S. Stankovich, D. A. Dikin, H. Liu, H. Shen, S. T. Nguyen, L. C. Brinson, *J. Polym. Sci. Part B: Polym. Phys*, 2007, 45, 2097.
19 X. S. Zhou, T. B. Wu, B. J. Hu, G. Y. Yang, B. X. Han,

Chem. Commun., 2010, 46, 3663.
20 R. Verdejo, M. Martin-Gallego, L. J. Romasanta, M. Hernández, M. M. Bernal, M. A. Lopez-Manchado, *J. Mater. Chem.*, 2008, 18, 2221.
21 X. Z. Zhou, X. Huang, X. Y. Qi, S. X. Wu, C. Xue, F. Y. C. Boey, Q. Y. Yan, P. Chen and H. Zhang, *J. Phys. Chem. C*, 2009, 113, 10842.
22 J. B. Liu, S. H. Fu, B. Yuan, Y. L. Li and Z. X. Deng, *J. Am. Chem. Soc.*, 2010, 132, 7279.
23 J. F. Shen, Y. Z. Hu, M. Shi, N. Li, H. W. Ma and M. X. Ye, *J. Phys. Chem. C*, 2010, 114, 1498.
24 A. Liu, T. Xu, J. Tang, H. Wu, T. Zhao, W. Tang, *Electrochim. Acta*, 2014,119, 43.
25 Y. Chu, Z. Wang, Q. Pan, *ACS Appl. Mater. Inter.*, 2014, 6, 8378.
26 M. Li, X. Bo, Z. Mu, Y. F. Zhang, L. Guo, *Sensor Actuat B-Chem.*, 2014, 192, 261.
27 L. Wang, J. H. Ma, *Acta. Phys-Chim. Sin.*, 2014, 30, 1267.
28 Y. H. Lu, M. Zhou, C. Zhang, Y. P. Feng, *J. Phys. Chem. C*, 2009, 113, 20156.
29 M. H. Yang, Y. H. Yang, Y. L. Liu, G. L. Shen, R. Q. Yu, *Biosens. Bioelectron.*, 2006, 21, 1125.
30 E. Antolini, T. Lopes, E. R. Gonzalez, *J. Alloy. Compd.*, 2008, 461, 253.
31 A. Hauch, A. Georg, *Electrochim. Acta*, 2001, 46, 3457.
32 E. Yoo, T. Okata, T. Akita, M. Kohyama, J. Nakamura, I. Honma, *Nano Lett.*, 2009, 9, 2255.
33 Y. M. Li, L. H. Tang, J. H. Li, *Electrochem. Commun.*, 2009, 11, 846.
34 S. Sharma, A. Ganguly, P. Papakonstantinou, X. Miao, M. Li, J. L. Hutchison, M. Delichatsios, S. Ukleja, *J. Phys. Chem. C*, 2010, 114, 19459.
35 C. Chen, M. Long, H. Wu, W. Cai, *Sci. China. Chem.*, 2013, 56, 354.
36 M. Q. Yang, X. Y. Pan, N. Zhang, Y. J. Xu, *Crystengcomm*, 2013, 15, 6819.
37 L. N. Zhang, H. H. Deng, F. L. Lin, X. W. Xu, S. H. Weng, A. L. Liu, X. H. Lin, X. H. Xia, W. Chen, *Anal. Chem.*, 2014, 86, 2711.
38 J. I. Paredes, S. Villar-Rodil, P. Solís-Fernández, A. Martínez-Alonso, J. M. D. Tascon, *Langmuir*, 2009, 25 5957.
39 S. Woo, Y.R. Kim, T. D. Chung, Y. Piao, H. Kim, *Electrochim. Acta*, 2012, 59, 509.
40 C. Chen, M. Long, H. Wu, W. Cai, *Sci. China. Chem.*, 2013, 56, 354.
41 J. Xu, Y. Li, J. Cao, R. Meng, W. Wang, Z. Chen, *Catal. Sci. Technol.*, 2015, 5, 1821.
42 J. I. Paredes, S. Villar-Rodil, A. Martınez-Alonso, J. M. D. Tascón, *Langmuir*, 2008, 24, 10560.
43 D. Li, M. B. Muller, S. Gilje, R. B. Kaner, G. G. Wallace, *Nat. Nanotechnol.*, 2008, 3, 101.
44 Y. Gao, L. Wu, K. Zhang, J. Xu, L. Lu, X. Zhu, Y. Wu, *Chinese Chem. Lett.*, 2015, 26, 613.
45 A. J. Bard, L. R. Faulkner, Wiley, New York, 1980.
46 E. Laviron, *J. Electroanal. Chem.*, 1974, 52, 355.
47 F. Anson, *Anal. Chem.*, 1964, 36, 932.
48 K. C. Lin, C. P. Hong, S. M. Chen, *Sensor. Actuat. B-Chem.*, 2013, 177, 428.
49 R. N. Goyal, M. Oyama, S. P. Singh, *J. Electroanal. Chem.*, 2007, 611, 140.
50 D. Boyd, J. R. B. Rodriguez, A. J. M. Ordieres, P. T. Blanco, M. R. Smyth, *Analyst*, 1994, 119, 1979.
51 Y. L. Wei, Q. Zhang, C. Shao, C. Li, L. P. Zhang, X. L. Li, *J. Anal. Chem.*, 2010, 65, 398.

Graphical Abstract

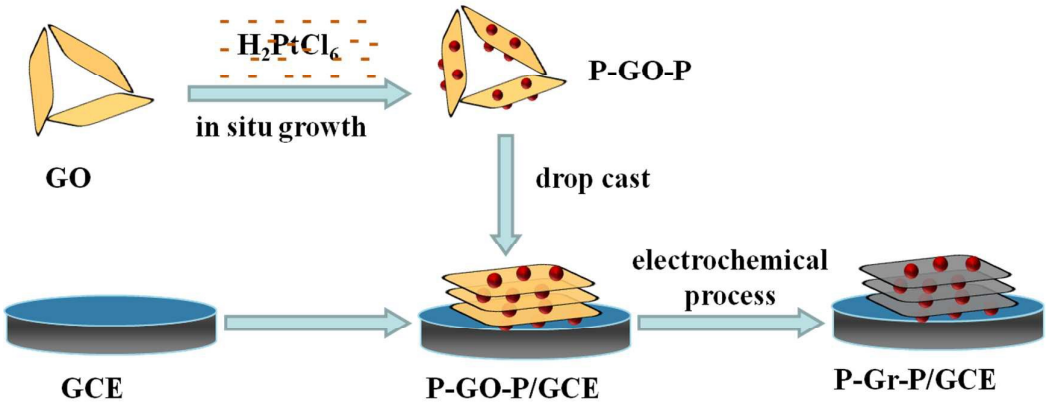

Sandwich-structured Pt-graphene-Pt was prepared by two step method including in situ growth and electrochemical reduction process.